

## The Sloan Digital Sky Survey-II: Photometry and Supernova Ia Light Curves from the 2005 data

Jon A. Holtzman,<sup>1</sup> John Marriner,<sup>2</sup> Richard Kessler,<sup>3,4</sup> Masao Sako,<sup>5,6</sup> Ben Dilday,<sup>3,7</sup>  
Joshua A. Frieman,<sup>2,3,8</sup> Donald P. Schneider,<sup>9</sup> Bruce Bassett,<sup>10,11</sup> Andrew Becker,<sup>12</sup>  
David Cinabro,<sup>13</sup> Fritz DeJongh,<sup>3</sup> Darren L. Depoy,<sup>14</sup> Mamoru Doi,<sup>15</sup>  
Peter M. Garnavich,<sup>16</sup> Craig J. Hogan,<sup>12</sup> Saurabh Jha,<sup>5,17</sup> Kohki Konishi,<sup>18</sup>  
Hubert Lampeitl,<sup>19,20</sup> Jennifer L. Marshall,<sup>14</sup> David McGinnis,<sup>3</sup> Gajus Miknaitis,<sup>3</sup>  
Robert C. Nichol,<sup>20</sup> Jose Luis Prieto,<sup>14</sup> Adam G. Reiss,<sup>19,21</sup> Michael W. Richmond,<sup>22</sup>  
Roger Romani,<sup>5</sup> Mathew Smith,<sup>20</sup> Naohiro Takanashi,<sup>15</sup> Kouichi Tokita,<sup>15</sup>  
Kurt van der Heyden,<sup>11,23</sup> Naoki Yasuda,<sup>18</sup> Chen Zheng<sup>5</sup>

---

<sup>1</sup> Department of Astronomy, MSC 4500, New Mexico State University, P.O. Box 30001, Las Cruces, NM 88003, holtz@nmsu.edu

<sup>2</sup> Center for Particle Astrophysics, Fermi National Accelerator Laboratory, P.O. Box 500, Batavia, IL 60510.

<sup>3</sup> Kavli Institute for Cosmological Physics, The University of Chicago, 5640 South Ellis Avenue Chicago, IL 60637.

<sup>4</sup> Enrico Fermi Institute, University of Chicago, 5640 South Ellis Avenue, Chicago, IL 60637.

<sup>5</sup> Kavli Institute for Particle Astrophysics & Cosmology, Stanford University, Stanford, CA 94305-4060.

<sup>6</sup> Department of Physics and Astronomy, University of Pennsylvania, 203 South 33rd Street, Philadelphia, PA 19104.

<sup>7</sup> Department of Physics, University of Chicago, Chicago, IL 60637.

<sup>8</sup> Department of Astronomy and Astrophysics, The University of Chicago, 5640 South Ellis Avenue, Chicago, IL 60637.

<sup>9</sup> Department of Astronomy and Astrophysics, The Pennsylvania State University, 525 Davey Laboratory, University Park, PA 16802.

<sup>10</sup> Department of Mathematics and Applied Mathematics, University of Cape Town, Rondebosch 7701, South Africa.

<sup>11</sup> South African Astronomical Observatory, P.O. Box 9, Observatory 7935, South Africa.

<sup>12</sup> Department of Astronomy, University of Washington, Box 351580, Seattle, WA 98195.

<sup>13</sup> Department of Physics, Wayne State University, Detroit, MI 48202.

<sup>14</sup> Department of Astronomy, Ohio State University, 140 West 18th Avenue, Columbus, OH 43210-1173.

<sup>15</sup> Institute of Astronomy, Graduate School of Science, University of Tokyo 2-21-1, Osawa, Mitaka, Tokyo 181-0015, Japan.

<sup>16</sup> University of Notre Dame, 225 Nieuwland Science, Notre Dame, IN 46556-5670.

<sup>17</sup> Department of Physics and Astronomy, Rutgers University, Piscataway, NJ08854.

<sup>18</sup> Institute for Cosmic Ray Research, University of Tokyo, 5-1-5, Kashiwanoha, Kashiwa, Chiba, 277-8582, Japan.

<sup>19</sup> Space Telescope Science Institute, 3700 San Martin Drive, Baltimore, MD 21218.

<sup>20</sup> Institute of Cosmology and Gravitation, Mercantile House, Hampshire Terrace, University of Portsmouth, Portsmouth PO1 2EG, UK.

<sup>21</sup> Department of Physics and Astronomy, Johns Hopkins University, 3400 North Charles Street, Baltimore, MD 21218.

<sup>22</sup> Physics Department, Rochester Institute of Technology, 85 Lomb Memorial Drive, Rochester, NY

## ABSTRACT

We present *ugriz* light curves for 146 spectroscopically confirmed or spectroscopically probable Type Ia supernovae from the 2005 season of the SDSS-II Supernova survey. The light curves have been constructed using a photometric technique that we call scene modelling, which is described in detail here; the major feature is that supernova brightnesses are extracted from a stack of images without spatial resampling or convolution of the image data. This procedure produces accurate photometry along with accurate estimates of the statistical uncertainty, and can be used to derive photometry taken with multiple telescopes. We discuss various tests of this technique that demonstrate its capabilities. We also describe the methodology used for the calibration of the photometry, and present calibrated magnitudes and fluxes for all of the spectroscopic SNe Ia from the 2005 season.

*Subject headings:* supernovae: general, techniques: photometric

## 1. Introduction

In its second phase of operations, the Sloan Digital Sky Survey (SDSS; York *et al.* 2000) telescope has been used to attack several different scientific programs. One of these is a supernova survey that ran from 1 September to 30 November for three years (2005-2007) and targetted Type Ia supernovae in the redshift range  $0.05 < z < 0.35$ . The project's scientific

---

14623-5603.

<sup>23</sup> Department of Astronomy, University of Cape Town, South Africa.

<sup>24</sup> Department of Astronomy, McDonald Observatory, University of Texas, Austin, TX 78712

<sup>25</sup> Apache Point Observatory, P.O. Box 59, Sunspot, NM 88349.

<sup>26</sup> Department of Astronomy, Seoul National University, Seoul, South Korea.

<sup>27</sup> Department of Astronomy, Columbia University, New York, NY 10027.

<sup>28</sup> Lowell Observatory, 1400 Mars Hill Rd., Flagstaff, AZ 86001

<sup>29</sup> Subaru Telescope, 650 N. A'Ohoku Place, Hilo, HI 96720

<sup>30</sup> Obserwatorium Astronomiczne na Suhorze, Akademia Pedagogiczna w Krakowie, ulica Podchorążych 2, PL-30-084 Kraków, Poland.

<sup>31</sup> Gemini Observatory, 670 North A'ohuoku Place, Hilo, HI 96720.

motivations are 1) to take advantage of the high areal coverage (over 150 square degrees per night) and moderate sensitivity ( $\sim 22$  mag) that can be obtained with the large format camera and drift scanning of SDSS to fill in a redshift regime where other surveys have not been efficient in finding supernovae, and 2) to take advantage of the well-understood photometric system of SDSS to minimize calibration errors and other systematics. An overview of the observational techniques and expected scientific returns of this program are given in Frieman *et al.* (2008).

Operationally, two strips (denoted strips 82N and 82S) located along the celestial equator with right ascension between 20h and 4h are monitored over a period of three months from September through November. These two strips, with a combined width of  $2.5^\circ$  and an area of approximately 300 square degrees, have been the subject of many previous SDSS imaging scans during the original SDSS survey. The SDSS SN survey alternates between these two strips on successive clear nights. There is a small overlap between the strips (roughly 10% of the area) to insure no sky coverage is lost. New transients and variable sources are identified by subtracting high signal-to-noise (S/N) template images constructed by coadding previous observations of the strip and inspecting the subtracted frames to find new objects. Candidate supernovae are identified via a combination of automated and interactive techniques, and observed spectroscopically using a variety of telescopes to confirm that they are supernova and to determine the supernova type and redshift. Details of the supernovae candidate identification and spectroscopic target selection are given in Sako *et al.* (2008); details of the spectroscopy and supernova typing are given in Zheng *et al.* (2008). The initial cosmological results from the SDSS-II Supernova Survey are presented in Kessler *et al.* (2009).

This paper presents the techniques used to measure the brightnesses of the supernovae for final analysis. We discuss the photometric calibration, photometric techniques, and expected errors in the resulting photometry, and present the resulting light curves for spectroscopically confirmed and likely type Ia supernovae from the first season (2005) of the SDSS-II Supernova Survey.

## 2. Data and data reduction

### 2.1. SDSS imaging

The imaging data are taken using the SDSS imaging camera (Gunn *et al.* 1998) on the SDSS 2.5m telescope (Gunn *et al.* 2006) at Apache Point Observatory (APO). This camera uses 30 imaging CCDs arranged in 6 columns; each column has a detector for each of the 5

SDSS filter bandpasses, *ugriz* (Fukugita *et al.* 1996). Additional detectors are used to assist with the astrometric calibration (Pier *et al.* 2003) of the science frames. The camera runs in drift scanning mode such that each column is exposed for 54 seconds per filter, with a slight time lag between successive filters. Operation of the camera for the SDSS-II supernova survey is identical to routine operation for the original survey (see Stoughton *et al.* 2002 and Adelman-McCarthy *et al.* 2008 for details of the survey operation and data releases).

The imaging data are processed through the standard SDSS processing pipeline, which uses the program PHOTO (Lupton *et al.* 2008) to remove instrumental signatures, flag bad pixels, determine a PSF, and create an object catalog with instrumental brightnesses. As output, PHOTO produces corrected frames, which have instrumental signatures removed and astrometric information in their headers, and mask frames that flag problematic pixels. Each column of a strip in the sky is divided into a series of adjacent fields ( $2048 \times 1489$  pixels, or roughly 800 by 600 arcsec), for output, with a small amount of overlap between fields.

For the purpose of identifying supernovae during the survey, template images from previous imaging scans are subtracted from the images from each supernova run. For the 2005 observing season, we used data from pre-2004 SDSS runs to create a coadded template. These coadded templates were constructed from a combination of between 4 and 9 photometric runs with good seeing. Before subtracting the template, a smearing kernel is applied to the template to match its PSF to the PSF of the supernova frame, and the template frame is astrometrically registered to the supernova frame. Details of the astrometric and PSF matching are given in an appendix in Sako *et al.* (2008). We refer to the resulting subtracted frames as the `Framesub` data. These data are used for identification of candidate supernovae, and for initial photometry that is used for target selection for spectroscopic followup; our final photometry, as discussed below, is more accurate, but is not used for target selection.

## 2.2. Other imaging

Additional imaging of SDSS-II SN candidates was obtained from several other telescopes: primarily, the 2.4m MDM telescope on Kitt Peak, the 88in UH telescope on Mauna Kea, and the ARC 3.5m and NMSU 1m telescopes at Apache Point Observatory. The main goals of these observations were to increase light curve coverage during periods of poor weather that limited the temporal coverage of the SDSS 2.5m data, to allow deeper observations for more distant SN and/or at later epochs than can be obtained with the fixed 54s integration time of the 2.5m telescope, and to measure the light curves of supernovae discovered late in the survey season into the month following the completion of the SDSS imaging. During the

2005 campaign, the APO weather was generally quite good, so these additional observations were not as critical as they might have been in poor weather.

On all of the non-SDSS telescopes, filter sets approximating the SDSS filter set were used, but there are still small but significant differences between the response functions. This is a serious issue for the supernova program, since we hope to reduce the systematic errors in the photometry to  $\sim 0.01$  magnitudes. In section 4.1.2, we discuss the techniques used to extract the supernova photometry from these other telescopes and the issues involved with using this photometry in a joint analysis with the 2.5m data.

### 3. Photometric calibration

The SDSS-II supernovae runs are taken on all fall nights during which the telescope can be operated, except for five nights around full moon. Much of the data is taken under non-photometric conditions. However, all of the data on strips 82N and 82S taken as part of the standard SDSS-I survey (before 2004) were taken under photometric conditions, with simultaneous monitoring of atmospheric transmission using the SDSS Photometric Telescope (PT). As a result, the standard SDSS-I imaging provides multiple photometric measurements of all stars along these strips. The details of the photometric calibration of the SDSS images is discussed in Hogg *et al.* (2001), Smith *et al.* (2002), Ivezić *et al.* (2004), and Tucker *et al.* (2006), and on the SDSS Web pages (<http://www.sdss.org>).

Ivezić *et al.* (2007) have taken the repeat observations along the equatorial strips and constructed a master catalog of standard stars in the SDSS system using these measurements. Variable stars are flagged by comparing the multiple measurements, and final median magnitudes for all non-variables with good S/N were compiled into the master catalog. A variety of tests with these measurements suggest that the catalog magnitudes are accurate to within  $\sim 0.01$  magnitudes.

We use the Ivezić *et al.* (2007) catalog to calibrate the supernovae frames. The details of which stars are used varies for the different photometric techniques, as discussed below, but in general, brightness measurements of a set of stars are made around each supernova candidate, and these measurements are compared with the catalog to determine photometric zeropoints for measurements of that candidate. Along with the derived zeropoints, the scatter of the observed star brightnesses relative to the catalog brightnesses are computed to determine how well single zeropoints match the frames; with the drift scanning that is used for the survey, stars at different right ascensions are observed over different time intervals, so the zeropoint can vary as a function of row position on the frames.

The number of calibration stars varies along the SDSS SN strip, largely due to the variation in Galactic latitude. The number of calibration stars around each supernova varies from a few to several hundred. However, in many cases, a large fraction of the calibration stars do not have  $u$ -band magnitudes in the calibration catalog, which limits our ability to extract  $u$ -band measurements for some objects.

Finally, the Ivezic *et al.* (2007) catalog does not quite extend to the western end of the supernova strip, in the first 10 degrees of the supernova strip, because only a smaller number of SDSS runs covered this area. In this region, we have constructed an analogous calibration catalog, but since it is based on fewer observations, the uncertainties in the calibration are a bit higher in this region.

### 3.1. Absolute flux calibration

The Ivezic *et al.* (2007) catalog is calibrated to the native SDSS survey photometric system. While this system was originally intended to be an AB system (Oke 1974, Fukugita *et al.* 1996), it was realized that the inclusion of the effects of atmospheric transmission make it differ slightly (at about a 4 percent level) from an AB system in the  $u$ -band; subsequent observations of calibrated targets suggest that, at the 1-2 percent level, the survey photometry may differ from that of a true AB system in the other bandpasses as well.

Various efforts have been made to understand the absolute calibration of the SDSS system. Here, we calibrate to the HST white dwarf system (Bohlin 2006). Bohlin (2001, 2004a, 2004b) present calibrated spectra for several white dwarfs and solar analog stars on this system. Unfortunately, all of these stars are too bright to be directly observed using the SDSS 2.5m telescope, and, in any case, none of them are in the region of the sky where multiple SDSS observations have been made. However, several of these stars have been observed numerous times by the SDSS Photometric Telescope (PT), which is normally used to transfer photometric zeropoints to data taken with the SDSS 2.5m telescope. While SDSS-like filters are used on the PT, the system response functions are not exactly the same between the two telescopes, so color terms have been determined to allow for the transformation of magnitudes observed on the PT to the SDSS system (which is defined as the system of the 2.5m telescope). These color terms have been defined over a relatively narrow range of color, corresponding to F and G type stars. As a result, while the color terms do not strictly apply to the white dwarf standards, the solar analog standards fall nicely within the color range for which the color terms have been determined.

There are three solar analogs for which 10 or more PT observations have been made:

P330E, P177D, and P041C. The observed PT measurements were transformed to the SDSS system using the standard survey color terms (Tucker *et al.*, 2006). These SDSS measurements were then compared with synthetic AB magnitudes calculated using the calibrated spectral energy distributions (SEDs) of the stars and the SDSS system response curves (from the SDSS web site, [www.sdss.org](http://www.sdss.org)). Differences between the synthetic and observed magnitudes are then interpreted to be the deviation of the SDSS system from a true AB system. The average magnitude offsets (AB-SDSS) for the three stars are determined to be  $-0.037$ ,  $0.024$ ,  $0.005$ ,  $0.018$ , and  $0.016$  mag for *ugriz*, respectively. Table 1 summarizes the observed and synthetic magnitudes for the solar analogs, and the average offsets; the offsets are defined such that they need to be added to the SDSS magnitudes to bring them onto an AB system.

We adopt these offsets for our supernova photometry, since accurate absolute calibration is important for cosmological analysis of the supernovae data. Note that these offsets rest on the assumptions of: 1) correct SEDs for the solar analogs, 2) correct observations of the solar analogs, 3) correct transformations of the observations to the SDSS system, and 4) correct knowledge of the SDSS system response.

We recognize that further refinements to the absolute calibration may be available in the future. We note that several other efforts have been made to understand the relation of the SDSS system to an AB system (see SDSS web site) that yield results similar, but not identical, to those adopted here. Differences in these analyses at the 1-2 percent level are consistent with our calibration error estimate of about 1%.

Because of potential refinements to the absolute flux calibration, we present two versions of supernova photometry for the data associated with this paper: magnitudes on the native SDSS system (no AB correction), and fluxes that have been determined using the AB corrections discussed above.

#### 4. Photometry methods

After the images are taken, initial, rapid photometry is required to identify candidates for spectroscopic followup (Sako *et al.* 2008). This quick photometry, which we call search photometry, measures SN brightnesses using a modified DOPHOT (Schechter, Mateo, & Saha 1993) technique on the pipeline template-subtracted frames. Each observation in each filter is processed independently. Objects are not required to be present at a common position in all filters and epochs and may be found in some filters but not others. The initial search photometry meets the goal of supernova detection and measurement (generally much better



than the 10% accuracy goal), but it does not provide the most accurate treatment of the data possible.

For the final photometry, we investigated three different techniques. The first, which we call forced photometry, also works on the template subtracted frames, but the photometry reduction forces the position of the supernova to be the same on all frames, where the forced position is determined from the average of the search photometry positions in frames where the SN is within 1 magnitude of its peak observed brightness. Forced photometry is used during the supernova search to obtain photometry on supernova candidates for epochs and filters in which an object was not detected by the initial photometry. For both search and forced photometry, the astrometric and photometric scalings of each frame are adopted from the `Framesub` software.

Two independent techniques that recompute the astrometric and photometric scalings, as well as provide independent photometry on the supernovae, were also developed. One, which we call “cross-convolution” photometry, measures stellar positions and intensities on search and template frames, and determines an astrometric solution and a photometric scaling. The template frame is convolved with the PSF of the search frame, and the search frame is convolved with the PSF of the template frame; this avoids the requirement of parameterizing the PSF as is done in frame subtraction pipeline. The convolved template frame is subtracted from the convolved search frame, and the magnitudes are determined by weighted PSF photometry on the difference, again requiring the same position for the supernova in all frames. The cross-convolution photometry uses PSFs as measured by the PHOTO pipeline.

Finally, we developed a technique that does not use template-subtracted frames, but instead fits all of the individual reduced frames with a model of the galaxy background and supernova; we call this technique “scene-modelling” photometry. Ultimately, we chose to use “scene modeling” as the final photometry because of its theoretical advantages, its superior ability to provide “smooth” supernova light curves, and accurate error estimates from first principles; no convolution or resampling of any image data is involved. Details of the technique are given in the next section. The other approaches are mentioned here to demonstrate that we made significant effort to determine the optimal photometry for the supernova light curve analysis.

#### 4.1. Scene modelling photometry

The main idea behind our scene modelling technique is to perform photometry on individual calibrated images without degrading the PSF and without any spatial resampling that leads to correlated noise between pixels. All of the frames are fit simultaneously with a model of the galaxy background plus supernova. This is statistically optimal in that the model produces a prediction for each observed pixel that can be compared to the observation and its error; propagation of pixel level errors to fitted quantities is made in a precise and rigorous fashion.

The basic concept is similar to the technique used by the Supernova Legacy Survey (SNLS; Astier *et al.* 2006), but developed independently, and includes a key new feature, namely, no spatial resampling. The photometry described in Astier *et al.* (2006) is accomplished by modeling each image as the sum of a time-independent galaxy background plus a time-dependent supernova and convolving the model with a separate PSF for each image; however, all images are resampled to a common pixel grid before doing the fit. This leads to correlated errors between adjacent pixels, which, as described by Astier *et al.*, lead to underestimated parameter uncertainties, including the uncertainty on the supernova flux measurements. Astier *et al.* estimate that the variances returned from the fit are 25% too small as a result of the pixel correlations. Because of this, they adopt empirical uncertainties derived from multiple observations on a given night. They find that the typical variances as derived from repeat observations are about 50% larger than those predicted from the fits. Our implementation does not involve any spatial resampling of the images, so there are no correlated errors that can cause derived errors to be underestimated. The tests described in Section 5 demonstrate that our error estimates are accurate.

We note that our technique provides the largest benefits when the pre-supernovae template images are of comparable (or lower) S/N to the supernovae images and/or the seeing in template images is worse than that of the images with the supernovae. If high S/N and good seeing template images are available, these can be resampled and degraded to the pointing and resolution of the supernovae frames without introducing too much correlated noise (because in this case the supernova frame, rather than the template, dominates the noise).

Aside from the modeling technique, our technique is customized for the SDSS survey to take advantage of the pre-existing photometric catalog of stars in the supernova fields.

We model each image as the sum of a set of stars, a galaxy, a supernova, and background. The galaxy is modelled as a grid of squares of constant surface brightness. The stars and supernova are modelled as point sources, with magnitudes that are time-independent and

time-dependent, respectively. A separate PSF is determined for each image, and each image is matched to the model convolved with the image’s PSF. A set of stars is used to determine the relative astrometric and photometric transformations between the frames, and the stars and supernovae are required to have the same relative positions in every frame.

The algorithm proceeds as follows. A set of calibration stars is extracted from our calibration star list around the position of each supernova. For each SDSS observation of each supernovae, a  $2048 \times 1024$  pixel image subsection ( $\sim 800 \times 400$  arcsec) is cut out of the PHOTO corrected frames in each filter, with the supernova centered in rows in the cutout (adjoining fields are pasted together if necessary). Hereafter, we refer to the image subsections as frames. Since the SDSS data is taken in drift-scanning mode, the mean time of observation differs by about 27 seconds from bottom to top of these image subsections. The calibration stars are sorted by brightness. Since the calibration stars only include non-variable stars and do not extend to the faintest stars in the frame, a star finding algorithm is used on a single  $g$ -band frame to obtain a more complete star list. Using this star list, any object from the calibration star catalog that has a nearby object is excluded, to ensure that the final calibration list contains only isolated stars.

For each frame, a slowly varying background model is derived by determining a sky value in 25 (a  $5 \times 5$  grid) subsections within the image. The sky level per pixel in each subregion is measured using an estimate of the modal value (Stetson 1987) in the region; the final sky level is remeasured after rejecting values  $5\sigma$  larger than the initial estimate (to further minimize effects of stars). A quadratic fit is done to these 25 values to provide a model of the sky background. The rms of the 25 independent measurements is compared with the standard deviation in the central region; if the variation across the entire frame is larger than expected from the individual variances, the frame is flagged as having a potentially uncertain sky level; the source of the variation in such frames can arise from rapid changes in atmospheric conditions, and, in some cases, from the presence of a very bright star in or near the image subsection. Only a small fraction of all of our images show this behavior.

On each frame, stars are identified using the DAOPHOT (Stetson 1987) FIND algorithm for potential use in determining the PSF; we use more than just calibration stars for this purpose since even variable stars are useful for PSF determination. This star list is filtered to remove all objects with nearby neighbors, and any objects with shape parameters that deviate significantly from those measured for the bulk of the stars. On each frame, aperture photometry measurements are made for the stars in the filtered list. A position independent PSF is created for the image frame using all stars within 3 magnitudes of the brightest star in the field. A constant PSF gives an adequate representation (in most cases) over the moderately small image subsection that we use. In any case, there are generally too few

stars to derive an accurate PSF model with spatial variation. The PSF representation is made using the PSF characterization of DAOPHOT (Stetson 1987): a Gaussian integrated over pixels is fit to the brightest PSF star, and the residuals from this Gaussian are stored in a lookup table at 0.5 pixel spacing. The removal of an underlying Gaussian minimizes the effect of interpolation errors in the lookup table. For any additional PSF stars, the integrated Gaussian from the brightest star is fit to each star individually, and the residuals are interpolated and added into the lookup table to reduce noise. The PSF is assumed to be zero beyond a specified PSF radius.

We then proceed to fit a model to the observed data. At each pixel with coordinates  $(x, y)$  and in a given filter, the model for the flux is given by:

$$M(x, y) = sky(x, y) + S \left( \sum_{stars} I_{star} PSF(x - x_{star}, y - y_{star}) + I_{SN} PSF(x - x_{SN}, y - y_{SN}) + \sum_{x_g, y_g} \mathcal{G}(x_g, y_g) PSF(x - x_g, y - y_g) \right) \quad (1)$$

where  $x$  and  $y$  are the horizontal and vertical pixel indices,  $M(x, y)$  is the total model intensity (DN) at each pixel,  $I_{star}$  is the known total calibrated brightness of each star,  $I_{SN}$  is the unknown total calibrated supernova intensity,  $PSF(\Delta X, \Delta Y)$  is the measured fraction of light from a star as a function of the distance of each pixel from the stellar position,  $\mathcal{G}(x_g, y_g)$  represents the unknown grid of galaxy intensities, and  $sky(x, y)$  is the measured background value at each pixel.  $S$  is the unknown frame scaling factor that converts the calibrated fluxes to DN on each individual frame. The positions  $(x_{star}, y_{star})$  and  $(x_{SN}, y_{SN})$  are the pixel coordinates of the stars and supernovae, which are derived from their celestial positions and an astrometric solution for each frame.

The fits are weighted by the expected errors from photon statistics and readout noise, using the gain ( $G$ ; the number of DN per detected photons) values for each camera column and each filter as given in the SDSS `fpAtlas` files. We adopted  $\sigma_{rn} = 5$  electrons for the readout noise; technically, the readout noise varies from chip to chip, but a single typical value was adopted since it is a negligible noise source. Specifically, we minimize:

$$\chi^2 = \sum_{xy} \frac{(O(x, y) - M(x, y))^2}{(M(x, y)/G + (\frac{\sigma_{rn}^2}{G^2}))} \quad (2)$$

where  $O(x, y)$  is the observed value at each pixel. Operationally, we limit the model to include stellar (and SN) flux out to a PSF radius of 5 arcsec from the center of each object.

Due to lower S/N in the outer regions of the PSF, only pixels within a specified fitting radius (which is taken as 3 arcseconds or the measured FWHM of the PSF, whichever is larger) are used in adjusting the fit parameters, but the contribution of objects out to 5 arcsec is included in the model.

Since the model is nonlinear in the fit parameters, the solution is iterated from a starting guess. Adjustments to the initial parameters are computed using the full Hessian matrix, using a Levenberg-Marquardt scheme. If the fit has abnormally large  $\chi^2$  after several iterations, the weight of pixels with large  $\chi^2$  ( $> 2.5\sigma$ ) is decreased; this attempts to prevent bad pixels from corrupting the fit quality. The fit is judged to converge when all of the point source intensities do not change significantly in an iteration.

The first step in solving for the model parameters is to determine accurate stellar positions for the stars on the calibration list. The initial positions from the calibration catalog are average positions from the pre-supernova template catalog. However, since the SDSS template images of the SDSS supernova survey area go back to 2001, proper motions are not negligible for some stars, and allowing for proper motions significantly improves the quality of the model fits to the data. Our first fit solves for stellar positions and proper motions using a subset of the SDSS  $r$ -band images. For this fit, we take the initial epoch and subsequent epochs separated by 60 or more days from the previous epoch. To maximize the baseline for proper motion determination, we use all SDSS data taken from the beginning of SDSS survey (2001) until the end of the SDSS SN survey (2007); this typically gives us 10-20 images to fit. The stack of image subsections is simultaneously fit for stellar positions (at epoch 2000), proper motions, an astrometric solution for each frame, and photometric frame scalings between the frames. We arbitrarily adopt the SDSS astrometric solution of the first frame in the list as the absolute reference frame, since all we really care about is accurate relative astrometry between the frames. This process yields us a list of stars with accurate relative positions on the sky, proper motions, and calibrated brightnesses. Since the fit only includes stars, the proper motions are not absolute, but are only relative (in the fit, we lock the proper motion of the first star to be zero); after the fit, we normalize them so that the mean proper motion of all of the stars is zero (but we allow for a proper motion of the reference frame in the galaxy fit, see below).

For the astrometric model, we adopt the distortion coefficients measured by the SDSS photometric pipeline, but solve for a full linear astrometric solution (6 parameters) within each of our subframes. For any frames where only 3 calibration reference stars are available, we constrain the astrometric solution to fit only 4 parameters for scale, rotation, and offset.

Given measured stellar positions, our second series of fits solves for the frame scale factors,  $S_{frame}$ , and the astrometric parameters for each frame. These can be determined for

each frame independently, since all of the stellar parameters (positions, proper motions, and intensities) are held fixed in the fit. Only frame parameters (which are independent from frame to frame) are solved for; in these fits, there are 7 parameters (6 linear astrometric parameters plus 1 photometric frame scaling). A single photometric frame scaling value for our subsections requires stable transparency over a time interval of  $\sim 81$  seconds, and over a spatial scale of  $\sim 800$  arcsec. Based on the residuals of stars across the field, we have found, to no surprise, that the assumption of a single photometric frame scale value becomes less accurate under cloudier conditions. As a result, we flag all frames where the photometric scaling is less than half the expected scaling for photometric weather (allowing for differences in airmass).

To identify frames that may have other problems, and to assess the quality of the astrometric/photometric solution, a final fit iteration is performed after the frame solution is determined; in this final iteration, we lock the frame parameters and stellar positions and fit for the individual stellar brightnesses. These recovered brightnesses are compared with the known brightnesses from the calibration star catalog. A subset of the best measured stars is selected so that it contains at least 5 stars (3 in the  $u$ -band). The mean magnitude difference, rms, and  $\chi^2$  for this set of stars are computed using the fit brightnesses and error estimates; for the  $\chi^2$  calculation, an error term is included for the uncertainties in the calibration magnitude of each star. The reduced  $\chi^2$  for the frame is recorded, and all frames with atypically large  $\chi^2$  are flagged. Finally, we estimate a “frame error” term by determining what additional error needs to be added (in quadrature) to bring the reduced  $\chi^2$  down to unity; this term is generally less than 0.01 mag, and is plausibly associated with errors that result from inaccuracies in the PSF model.

Figure 1 shows the difference of the recovered stellar magnitudes and the calibration magnitude for all of the calibration stars for all of the 2005 confirmed type Ia supernovae as a function of stellar brightness and color. These plots demonstrate that we accurately recover the brightnesses of the calibration stars with our PSF fitting, and display the typical photometric errors in our exposures as a function of stellar magnitude.

The derivation of astrometric parameters and photometric scaling factors for each of the supernovae frames discussed so far is similar to what is done for most supernovae surveys, although the inclusion of proper motions may not be typical (or needed, when the time baseline is short). We also have attempted to do a careful accounting of errors.

In the third, and final, fitting stage, we extract a small  $128 \times 128$  ( $\sim 50 \times 50$  arcsec) image subsection around the position of the supernova in every frame. Using the derived frame photometric scalings and astrometry, we simultaneously fit the entire stack of images (all epochs and all filters) to solve for a temporally constant galaxy plus a temporally variable

supernova. Frames that have been flagged as potentially unreliable in any of the previous steps are not allowed to influence the galaxy model, but are still included for a determination of the supernova brightness (as described below, the flag is carried along for the final output). We obtain the estimated supernova peak intensity date from the search photometry, and force all observations more than 90 days before peak to have zero supernova flux. For a typical supernova, the image stack contains several hundred images: 10-20 pre-SN images and 10-20 SN images in each of 5 filters. A single supernova position is fit to the entire stack. The galaxy is modelled as a grid of squares of constant surface brightness; we use a 15 by 15 grid of 0.6 by 0.6 arcsec squares, with independent brightnesses in each of the 5 filters at each location. The model galaxy size of 9 by 9 arcsec around the position of the supernova may not model the entire galaxy, but models a sufficient amount to determine the galaxy contribution at the position of the supernova even under the worst seeing conditions. The galaxy model is interpolated to the pixels on each frame separately; the choice of the model grid spacing is not critical. Given the typical SDSS seeing of  $\sim 1.2$  arcsec, it is clear that the information at the 0.6 arcsec scale is limited, and in fact, the recovered galaxy maps often do not show realistic structure at this spatial scale. However, when the recovered maps are smoothed to the typical seeing, they match the observed galaxy well, and the relatively fine sampling allows us to match regions with steep intensity gradients. We have investigated using both coarser and finer samplings for the galaxy model, and find that the supernova photometry is relatively insensitive to sampling changes. The supernova is allowed to have a separate brightness in each frame, but is required to have a common position in *all* frames; the position is iteratively determined by the fit using all of the available data. The total number of fit parameters in the final fit is

$$N_{fit} = (15 \times 15)N_{filt} + N_{epoch} * N_{filt} + 4 \tag{3}$$

where  $N_{filt}$  is the number of filters (usually 5, but sometimes 4 if there are an insufficient number of *u*-band calibration stars) and  $N_{epoch}$  is the number of epochs observed later than 90 days before the estimated SN peak. The final four parameters are for the celestial position  $(\alpha, \delta)$  of the supernova, and the mean proper motion of all of the calibrating stars in the field; it is the galaxy light that constrains the mean proper motion of the calibration stars. <sup>1</sup>

Output from the final fit includes supernova brightnesses for each frame along with error estimates from the least-squares fit. Since the noise model is derived from photon statistics and readout noise, but does not include terms from an imperfect PSF, inaccuracies in the

---

<sup>1</sup>For hostless supernovae, the mean proper motion would be unconstrained, but for such objects, there is no pre-SN galaxy background that needs to be accounted for, and proper motions are negligible over the decay time of the supernova.

determination of the frame photometric zeropoints, or sky model, the least-squares errors may be underestimated, especially for the brightest points where statistical errors are small. In an attempt to provide realistic error estimates for all points, we take the errors from the fit and add in the individual “frame errors”, the derivation of which was previously described. Since these are derived from observations of relatively bright stars, they are expected to account for errors in PSF modelling and frame scaling.

Two other sources of error are also considered: error arising from inaccuracies in the sky estimate and error from inaccuracies in the galaxy model at the location of the supernovae. The former gives a systematic error over the pixels covered by a supernova at any individual epoch, but is likely to be a random error source for different supernovae epochs. The galaxy model error gives systematic errors that are similar (not identical, because of seeing variation) for all epochs of a given supernova. We estimate the sky error based on the variation of sky level from different subsections of the frame (although in cases where there is real structure in the sky background, this might overestimate the sky error). The galaxy error is calculated from the least squares fit, and includes correlated errors which exist between adjacent locations in the galaxy model, since this model is sampled finer than the point spread function; this estimate of the galaxy error may be an underestimate since it does not account for errors that would result from systematic errors in the astrometric solution of the frames. Since the portion of the galaxy that contributes flux at the location of the supernova depends on the seeing, the galaxy error can vary from frame to frame; for output, we calculate a typical galaxy error that arises for a seeing of 1.2 arcsec. The estimated errors from inaccuracies in sky and galaxy subtraction are output, along with the supernova brightness and its random error. Clearly, the importance of the sky and galaxy subtraction errors is larger when the supernova brightness is comparable or fainter than the sky or galaxy. In general, errors in the sky background dominate those in the galaxy model.

We have created images of the frame with the model subtracted, and inspection of these provide qualitative confirmation the quality of the model (see below for some quantitative tests).

Figures 2 and 3 show an example of the procedure applied to one measurement of one of our supernovae. Figure 2 demonstrates the initial astrometric and photometric solution that is determined for each frame individually. The left image shows the image subsections that is used; circles show the calibration reference stars, and the square shows the supernova. The right image shows the same frame after the best fit model has been subtracted. Figure 3 shows the region around the supernova that is used to simultaneously solve for galaxy background, supernova position, and supernova brightness at each epoch; in this stage, an entire stack of these images is fit simultaneously.



We note that the scene modelling technique does not require perfect spatial overlap between all of the images, so long as there are some stars in common in all of the frames to allow determination of accurate relative astrometry. For supernova that lie in the overlap between strips 82N and 82S, there may be few, if any, reference stars in common between the northern and southern strips. In these cases, the entire dataset is still fit simultaneously. However, the final iteration allows for a global shift between all of the frames in one strip to those in the other strip; similarly, the two strips are allowed to have different mean stellar proper motions. It is the galaxy itself that provides the information to determine the global shift and proper motion difference between the two strips.

#### 4.1.1. Data flags

For each supernova measurement, we set a flag to allow for points of potentially poorer quality to be recognized. The value of the flag is a bitwise combination of multiple criteria:

- 1 Sky brightnesses more than twice median sky brightness from entire stack of images in this filter, *i.e.* , moon or clouds
- 2 FWHM of stellar images larger than 2 arcsec, *i.e.* , poor seeing
- 4 photometric scale factor less than 0.5, *i.e.* , moderately cloudy conditions
- 8 atypical sky variation: ratio of sky variation between image subsections to sky variation within a subsection significantly larger than median of entire stack in this filter (can arise in cloudy conditions)
- 16 large sky variation: ratio of sky variation between image subsections large compared with sky variation within a subsection (can arise from presence of bright star nearby)
- 32 derived supernova brightness fainter than underlying galaxy brightness (measured using the PSF of the frame)
- 64 Fewer than 5 calibration stars on frame
- 128 rms photometry of calibration stars atypically large
- 256 fit exceeded maximum number of iterations, or fit quality (from individual frame  $\chi^2$  ) poorer than typical
- 512 No calibration stars

1024 Photometric scale factor so low, rms photometry of calibration stars so high, variation in sky brightness so high, frame fit quality so poor, or global fit quality so poor, to strongly suggest that data should not be used, i.e. **bad data**.

The highest quality points have a flag value of 0. Flag bits of 1,2,3,8,16,64, and 128 are determined from the individual frame fits before the global galaxy/supernova solution is determined. Frames with any of these flags set are not used to influence the galaxy model in the final fit, with the exception of flag=16. This flag can be set because of background light from a nearby very bright star. In this case, the problem persists at all epochs, and a result can be obtained only if these frames are used.

Most points with  $0 < flag < 1024$  appear to be of good quality judging from how well they fit on the light curves. Bit 6 (32) flags points where the supernova is fainter than the underlying galaxy, and as a result, applies to many points for objects buried within bright hosts and to many late time points. These are the points that are most sensitive to the accuracy of the galaxy model, and are most subject to the possibility of systematic error.

Observations with the 1024-bit set, i.e.  $flag > 1024$  are generally unusable, and should not be trusted. For applications where only the cleanest (potentially highest accuracy) data are desired, even at the expense of throwing away many apparently good points, one might choose to only use points with  $flag = 0$ . The SDSS cosmology analysis (Kessler *et al.* 2009) uses essentially all points with  $flag < 1024$ .

#### 4.1.2. Including non-2.5m data in scene modelling

An important feature of the scene modeling technique is that the model is independent of telescope characteristics such as pixel size and registration relative to the model. It is therefore straightforward to combine data from different telescopes in the same fit. The same catalog stars can be used to calibrate the response of all the telescopes.

In general, each telescope will have its own unique set of filter response curves. As a result, relative photometry of objects with different spectral energy distributions will differ from telescope to telescope. If the differences in filter response from telescope to telescope are small, then the differences can be parameterized by use of a linear color term. For the non-2.5m data, when deriving the photometric scaling for each frame from the calibration stars, we allow for a color term to be fit as well as a photometric zeropoint. Since we expect the color term to be constant in time, at least over an observing season, we adopt an average color term from the photometric solutions for all frames in a given filter using all of the supernovae observed in the 2005 season; this allows for a large range of stellar colors to be

sampled.

For the 2005 season, photometry of the SDSS supernovae was obtained with several other telescopes; in most cases, only 4-color (*griz*) observations were obtained. Each individual frame was fit to the calibration star list derived from the SDSS frames exactly as above, except a color term was included when fitting the instrumental brightnesses to the catalog brightnesses. For each telescope, color terms of the form

$$g = g_{obs} + t_g(g - r) \tag{4}$$

$$r = r_{obs} + t_r(r - i) \tag{5}$$

$$i = i_{obs} + t_i(r - i) \tag{6}$$

$$z = z_{obs} + t_z(i - z) \tag{7}$$

were determined, requiring time-independent transformation coefficients over the length of the observing season.

Figure 4 shows an example of the photometric calibration results for all of the stars on MDM 2.4m frames from the 2005 season after the derived color terms have been removed; this plot is equivalent to Figure 1 for the SDSS frames. The adopted color equations (that are applied for this plot) are:

$$g = g_{mdm} - 0.1(g - r) \tag{8}$$

$$r = r_{mdm} - 0.05(r - i) \tag{9}$$

$$i = i_{mdm} + 0.08(r - i) \tag{10}$$

$$z = z_{mdm} \tag{11}$$

Similar relations have been derived for the other telescopes used during the survey.

The differing filter responses also affect the underlying galaxy background. To account for this, we apply the stellar color term to the underlying galaxy model as well. The accuracy of the application of a color term depends on the degree to which the spectral energy distribution of the object to which the color term is applied (the galaxy, in this case) is similar to the SED of the objects (stars, in this case) used to derive the color term. While SEDs of galaxies are not identical to those of stars, at the moderate redshifts considered here, they are not dramatically different. Combined with the fact that the color terms are relatively small (since SDSS-like filters were used on all of the non-2.5m telescope), we feel confident that the application of the stellar color terms to the galaxy background model is adequate.

For the final supernova photometry, the non-2.5m frames can be included in the final photometry iteration described above. However, to ensure that any issues with the photometric transformation for the non-2.5m data do not deteriorate the quality of the SDSS

2.5m photometry, we do not allow the non-2.5m data to contribute to the solution of the galaxy model itself; only 2.5m data is used to constrain this model, and the inclusion (or lack thereof) of non-2.5m data has no effect on the 2.5m photometry.

Interpreting the supernova photometry from the non-2.5m data can be challenging, because supernovae have spectral energy distributions that are quite different from stars. As a result, application of color terms derived from stars does not necessarily bring supernova photometry onto the 2.5m system. Clearly, the use of these data in conjunction with the 2.5m photometry requires some understanding of the response differences between the telescopes and the spectral energy distribution of the supernovae at different epochs (*e.g.*, via so-called S-corrections).

Unfortunately, it is usually rather difficult to get accurate measurements of the response functions of different systems. For some of the telescopes we have obtained synthetic response functions from combinations of response functions of individual components. However, color terms computed from application of these response functions with libraries of stellar spectral energy distributions do not always match the measured color terms, suggesting errors in the response functions or the stellar libraries. This suggests that extreme caution should be used when applying products of individual component responses to determining transformations between observations using different photometric systems. We plan to investigate this in detail using measured response curves, the stellar calibration data, and several near-simultaneous observations of supernovae by multiple telescopes.

Since the weather at APO was quite good for the 2005 season, the 2.5m light curves provide good coverage even without the non-2.5m data. Because of this and the complication of understanding the system responses of the non-2.5m data, we have chosen not to include these data in our initial analyses, and in the data release described in this paper. However, we hope to do so in the future, especially since we expect the other telescopes to contribute more in the last two observing seasons, mostly through followup of objects discovered late in the 2.5m observing season; in 2005, many of the late objects do not have sufficient coverage to make them useful. It is in anticipation of using these data that we have included the discussion of the application of scene modelling to non-2.5m data here.

## 5. Photometry tests

We have performed a number of exercises to verify and improve the quality of the scene modelling photometry and error estimates. These tests also allow us to make educated decisions about what, if any, data cuts should be made before light curve analysis.

### 5.1. Stellar photometry

The first test treats real stars nearby the supernovae as if they were supernovae themselves, recovers light curves for them, and compares the derived brightnesses with the standard star catalog brightnesses. Using stars near the supernova allows us to accurately understand how any errors in astrometry and the PSF are likely to affect the supernova photometry. Unlike supernovae, there is no galaxy background underneath these stars, but fitting for a model background that is zero is a valid, if somewhat unrealistic, test. In order to simulate an underlying zero galaxy background, we remove the star from the early epoch frames by replacing it with sky background taken from a nearby region of blank sky. The full stack of images (including the early epochs with star removed, and later epochs with star retained) was then run through the scene modelling software, allowing for a background to be fit.

Note, however, that the “known” calibration magnitudes (taken from Ivezic et al. 2007) are actually not *perfectly* known, and any errors in these will lead to increased scatter in our comparison (which includes many stars). To compensate for this, we have averaged all of our measurements of these stars (which make for many more measurements than went into the Ivezic et al. catalog!), and compare the individual measurements against this refined average.

Results are shown in Figure 5. The left panel plots the error in recovered brightnesses as a function of the stellar brightness. The central panel gives a histogram of the difference (standard - observed). In general the recovered brightnesses are, to within estimated errors, consistent with the known brightness, with median errors from the entire sample of stars of only a few millimag.

The right panel shows the histogram of the difference normalized by the calculated error; if the error estimates were perfect, this should be a Gaussian of unit width. A more quantitative analysis of the error estimates is given in Figure 6, which shows the calculated reduced  $\chi^2$  from these distributions. For the brighter stars, the reduced  $\chi^2$  are near the expected value of unity for some filters, but they are a bit too large for other filters. We have investigated the source of this, and find that the larger  $\chi^2$  come mostly from points with small predicted errors, less than 0.01 mag. This suggests that even with our procedure of adding a frame error, we still slightly underestimate our errors for the brightest sources. If we were to impose a 0.01 mag floor on the predicted errors, the  $\chi^2$  for the stars comes down near unity in most cases. We note that our supernovae are essentially never so bright as to have such a small error. For the fainter stars, the  $\chi^2$  values are slightly too large in the  $r$  and  $i$  filters. This likely arises because no sky error has been included in these error estimates (see section 5.3).

## 5.2. Pre-supernovae measurements

To test for errors in modelling a real underlying galaxy background, we measured the supernovae flux for real supernovae at epochs before the supernova actually occurred, to see how well we would recover zero flux. Clearly, the galaxy model depends on the pre-SN epochs and the quality of that model will deteriorate if we remove too many of the pre-SN epochs from the list of images with constrained zero supernovae flux. Because of this, we chose to do this test using the 2005 data, but looking at locations where supernovae were discovered in 2006. This provides a good representation of the real situation for the 2005 supernovae.

Figure 7 shows the results for measurements at the location of the 2006 supernovae in the 2005 data. The ideal situation is to measure identically zero supernova flux. The left panel shows the histogram of the difference between the observed and zero flux, in units of microJansky ( $1\mu Jy = 10^{-29} \text{ ergs/cm}^2/\text{s/Hz}$ ; a source with apparent magnitude of 20 has a flux of  $36.31 \mu Jy$ ). The right panel shows the histogram of the magnitude difference normalized by the predicted error. While there are a few points with measured brightness significantly different from zero, the bulk of the distribution follow the expected normal distribution. A more quantitative discussion of the estimated errors is presented in the following section.

## 5.3. Artificial supernovae

Finally, to test the accuracy of photometry at low flux levels against the galaxy background, we inserted artificial point sources into the frames and measured their brightnesses. Again, we used the locations of the 2006 supernovae to place artificial sources into the 2005 frames. We inserted artificial supernovae at 11 different flux levels. To reduce computation time, we split the 2006 sample of about 250 supernovae locations into 11 groups, so at each level, we inserted artificial objects about 22 different sky locations; at each location, artificial objects were placed in about 20 different epochs in the 2005 observations.

Artificial supernovae tests are not perfectly realistic because one must assume an astrometric solution, a photometric solution, and a PSF to insert the artificial objects, and usually the same quantities are used in the data reduction. For situations where uncertainties in any of these are the dominant source of error (bright objects), artificial supernovae tests are likely to provide overly optimistic results. As a result, we performed these tests only at a range of low flux levels. Artificial supernovae were placed into the frames using the derived astrometric solution and photometric scalings, and the measured PSF. The entire stack of

images was then run through the scene modelling software, and the measurements at the supernova position were compared with the known artificial supernovae brightnesses.

For each artificial supernova test, we computed the median flux offsets between the measured and the input value, and calculate the mean fractional error of the recovered measurements. These are shown in the top panel of Figure 8 as a function of the input brightness. The error bars are the computed error of the median values, given the sample size. One can see that the flux is recovered accurately: to within a percent except for the faintest objects (and possibly even for these, given the statistical errors). The few points that deviate the farthest from a mean error of zero generally include locations where the artificial star was placed at a location with a bright galaxy background (*i.e.* in the center of a galaxy). It is clear that this is the most challenging situation for accurate recovery of a supernova brightness; if the background is very bright, errors in the astrometry or PSF can throw off the recovered supernova brightness.

Note that the error bars shown are the error of the sample mean; the statistical error on individual measurements are much larger than any small residual bias. This is demonstrated in the middle panel, which shows the mean of the error in recovered magnitude, normalized by the error estimate.

The bottom panel of Figure 8 shows a reduced  $\chi^2$  value, calculated from the square of the difference between recovered and input magnitude, normalized by the estimated variance. If our error estimates are perfect, these should have values near unity. The open points show  $\chi^2$  as computed using the random error on the derived intensities; in general, these are slightly larger than unity. However, if one adds in quadrature the systematic errors from the sky determination (which should be random over a set of observations on different dates), then one gets the  $\chi^2$  values shown with the filled points. These show that using error estimate based on a combination of the flux plus sky error gives accurate error estimates, although our estimate of the sky error may be slightly too large.

## 6. Light curves

In the 2005 SDSS SN season, 130 type Ia supernovae were spectroscopically confirmed, along with an additional 16 spectroscopically probable Type Ia's. A complete list of all of the discovered supernovae, along with positions and IAU designations, including non-Ia supernovae, is presented in Sako *et al.* (2008).

We have used scene modelling to derive light curves for the 146 objects; the photometry data is available in the electronic version of this paper. Table ?? shows a portion of a sample

data table for one of our supernovae, SN2005hk, which has been discussed by Phillips *et al.* (2007). The files contain several lines of header information about the object: the SDSS internal candidate ID number, the IAU designation, the position, SDSS type, and redshift. In addition, approximate underlying galaxy surface brightnesses in each bandpass are given, as determined by the scene modelling photometry. The epoch of each observations is given as a modified heliocentric Julian date. The magnitudes in the file are given as asinh magnitudes (Lupton *et al.* 1999) on the native SDSS photometric system, using the softening parameters given in Stoughton *et al.* (2002). The fluxes are given in units of microJanskys, using the corrections to an AB system described in Section 3.1; by definition, an object with an AB magnitude of zero and flat  $F_\nu$  spectrum has a flux of  $3.631 \times 10^9 \mu Jy$ . Although no extinction correction has been applied to the measured brightnesses, the Galactic extinction as estimated from the Schlegel, Finkbeiner, & Davis (1998) maps is given in the file headers. The spectroscopic observations and the determination of the redshifts are described in Zheng *et al.* (2008). The redshifts, which were obtained by a variety of telescopes (Hobby-Eberly Telescope, Apache Point Observatory 3.5-m, Subaru Telescope, William Herschel Telescope, Nordic Optical Telescope, ESO New Technology Telescope, WIYN Telescope, Keck Observatory, and the South African Large Telescope), are in the heliocentric frame.

In Figure 9, we show our derived light curves for the 146 supernovae, sorted in order of redshift. These demonstrate the quality of the light curves. The plots include information about the IAU designation of these supernovae, and also give the estimated  $r$ -band galaxy surface brightness (from the scene modelling results) at the location of the supernova.

## 7. Conclusion

We have presented a general technique, scene-modelling photometry, for extracting supernovae photometry from multiple observations. A key feature of this technique is that it does not require resampling of data, resulting in accurate photometry and error estimates. Fitting all of the images as a sum of supernova and galaxy light results in optimal use of all of the data, giving the highest precision in the determination of the supernova light curves. Another important consequence of this technique is that it is straightforward to combine data from several pointings or even telescopes, although the existence of non-zero color terms between different telescopes remains a limitation in the accuracy of the photometry.

We use the technique to extract photometry for all of the confirmed and probable type Ia supernova candidates from the 2005 SDSS SN season. All of the data is accessible for public use via electronic tables and will also be available through the SDSS supernova web site. These data provide the basis for the initial analysis of the SDSS supernova survey.



Funding for the creation and distribution of the SDSS and SDSS-II has been provided by the Alfred P. Sloan Foundation, the Participating Institutions, the National Science Foundation, the U.S. Department of Energy, the National Aeronautics and Space Administration, the Japanese Monbukagakusho, the Max Planck Society, and the Higher Education Funding Council for England. The SDSS Web site is <http://www.sdss.org/>. This work was also partially supported by Los Alamos National Laboratory University of California Directed Research and Development Fund. The Hobby-Eberly Telescope (HET) is a joint project of the University of Texas at Austin, the Pennsylvania State University, Stanford University, Ludwig-Maximilians-Universität München, and Georg-August-Universität Göttingen; the HET is named in honor of its principal benefactors, William P. Hobby and Robert E. Eberly.

The SDSS is managed by the Astrophysical Research Consortium for the Participating Institutions. The Participating Institutions are the American Museum of Natural History, Astrophysical Institute Potsdam, University of Basel, Cambridge University, Case Western Reserve University, University of Chicago, Drexel University, Fermilab, the Institute for Advanced Study, the Japan Participation Group, Johns Hopkins University, the Joint Institute for Nuclear Astrophysics, the Kavli Institute for Particle Astrophysics and Cosmology, the Korean Scientist Group, the Chinese Academy of Sciences (LAMOST), Los Alamos National Laboratory, the Max-Planck-Institute for Astronomy (MPA), the Max-Planck-Institute for Astrophysics (MPiA), New Mexico State University, Ohio State University, University of Pittsburgh, University of Portsmouth, Princeton University, the United States Naval Observatory, and the University of Washington.

## REFERENCES

- Adelman-McCarthy, J., *et al.* 2008, ApJS, 175, 297
- Astier, P. *et al.* , 2006, A&A, 447, 31
- Frieman, J. *et al.* , 2008, AJ, 135, 338
- Fukugita, M., Ichikawa, T., Gunn, J.E., Doi, M., Shimasaku, K., and Schneider, D.P. 1996, AJ, 111, 1748
- Gunn, J., *et al.* , 1998, AJ, 116, 3040
- Gunn, J.E., *et al.* 2006, AJ, 131, 2332
- Hogg, D.W., Finkbeiner, D.P., Schlegel, D.J., and Gunn, J.E. 2001, AJ, 122, 2129
- Ivezic, Z., *et al.* 2004, AN, 325, 583

- Ivezic, Z., Smith, J.A., Miknaitis, G., Lin, H., Tucker, D., Lupton, R., Knapp, G., Gunn, J., Strauss, M., Holtzman, J., Kent, S., Yanny, B., Schlegel, D., Finkbeiner, D., Padmanabhan, N., Rockosi, C., Juric, M., Bond, N., Lee, B., Jester, S., Harris, H., Harding, P., Brinkmann, J., York, D., for the SDSS Collaboration, 2007, ApJ, 134, 973
- Kessler, R. et. al., 2009, Accepted by ApJS (arXiv:astro-ph/0909.xxxx)
- Lupton, R.H., Gunn, J.E., and Szalay, A.S. 1999, AJ, 118, 1406
- Lupton, R., et. al., 2008, in preparation
- Oke, B. 1974, ApJS27, 21
- Pier, J.R., Munn, J.A., Hindsley, R.B., Hennessy, G.S., Kent, S.M., Lupton, R.H., and Ivezic, Z. 2003, AJ, 125, 1559 (Astrometry)
- Sako, M. et. al., 2008, AJ, 135, 348
- Schechter, P.L. , Mateo, M, & Saha, A. 1993, PASP105, 1342
- Schlegel, D., Finkbeiner, D., & Davis, M., 1998, ApJ, 500, 525
- Smith, J.A., *et al.* 2002, AJ, 123, 2121 (Photometric System)
- Stetson, P.B., 1987, PASP, 99, 191
- Stoughton, C., *et al.* 2002, AJ, 123, 485 (Early Data Release)
- Tucker, D., *et al.* 2006, AN, 327, 821 (MT Pipeline)
- York, D.G., *et al.* 2000, AJ, 120, 1579 (Technical Summary)
- Zheng, C. et. al., 2008, AJ, 135, 1766

Table 1. Observed and synthetic measurements of solar analogs

| star                                | <i>u</i> | <i>g</i> | <i>r</i> | <i>i</i> | <i>z</i> |
|-------------------------------------|----------|----------|----------|----------|----------|
| Observed mags (transformed to SDSS) |          |          |          |          |          |
| P330E                               | 14.548   | 13.280   | 12.841   | 12.701   | 12.674   |
| P177D                               | 15.118   | 13.745   | 13.300   | 13.158   | 13.125   |
| P041C                               | 13.573   | 12.260   | 11.844   | 11.719   | 11.703   |
| Synthetic mags                      |          |          |          |          |          |
| P330E                               | 14.506   | 13.303   | 12.839   | 12.708   | 12.675   |
| P177D                               | 15.085   | 13.776   | 13.307   | 13.178   | 13.142   |
| P041C                               | 13.537   | 12.279   | 11.852   | 11.746   | 11.732   |
| Differences ( $m_{syn} - m_{obs}$ ) |          |          |          |          |          |
| $\Delta m$                          | -0.037   | 0.024    | 0.005    | 0.018    | 0.016    |
| rms $\Delta m$                      | 0.005    | 0.006    | 0.005    | 0.010    | 0.014    |

Table 2. Photometry for SN 2005hk (SDSS SN 8151)

| FLAG <sup>a</sup> | MJD         | FILT <sup>b</sup> | MAG <sup>c</sup> | MERR <sup>d</sup> | MSERR <sup>e</sup> | MGERR <sup>f</sup> | FLUX <sup>g</sup> | FLUXERR <sup>h</sup> | SERR <sup>i</sup> | GERR <sup>j</sup> | NPRE <sup>k</sup> | TELE | RUN <sup>l</sup> | STRIP <sup>m</sup> |
|-------------------|-------------|-------------------|------------------|-------------------|--------------------|--------------------|-------------------|----------------------|-------------------|-------------------|-------------------|------|------------------|--------------------|
| 0                 | 53671.34315 | 1                 | 18.745           | 0.012             | 0.001              | 0.001              | 1.128E+02         | 1.247E+00            | 1.479E-01         | 9.707E-02         | 10                | sdss | 5786             | 82S                |
| 0                 | 53671.33983 | 2                 | 18.960           | 0.018             | 0.005              | 0.001              | 9.419E+01         | 1.562E+00            | 4.341E-01         | 1.051E-01         | 12                | sdss | 5786             | 82S                |
| 0                 | 53671.34066 | 3                 | 19.288           | 0.023             | 0.003              | 0.002              | 6.880E+01         | 1.458E+00            | 2.055E-01         | 1.349E-01         | 12                | sdss | 5786             | 82S                |
| 0                 | 53671.34232 | 4                 | 19.609           | 0.096             | 0.066              | 0.012              | 5.115E+01         | 4.547E+00            | 3.125E+00         | 5.661E-01         | 12                | sdss | 5786             | 82S                |
| 0                 | 53671.34149 | 0                 | 18.612           | 0.035             | 0.003              | 0.003              | 1.349E+02         | 4.349E+00            | 3.877E-01         | 3.688E-01         | 10                | sdss | 5786             | 82S                |
| 0                 | 53674.24276 | 1                 | 16.989           | 0.012             | 0.000              | 0.000              | 5.686E+02         | 6.285E+00            | 1.035E-01         | 9.707E-02         | 10                | sdss | 5797             | 82S                |
| 0                 | 53674.23944 | 2                 | 17.103           | 0.006             | 0.000              | 0.000              | 5.210E+02         | 2.879E+00            | 1.724E-01         | 1.051E-01         | 12                | sdss | 5797             | 82S                |
| 0                 | 53674.24027 | 3                 | 17.352           | 0.009             | 0.001              | 0.000              | 4.093E+02         | 3.393E+00            | 4.193E-01         | 1.349E-01         | 12                | sdss | 5797             | 82S                |
| 0                 | 53674.24193 | 4                 | 17.576           | 0.017             | 0.004              | 0.002              | 3.336E+02         | 5.224E+00            | 1.132E+00         | 5.661E-01         | 12                | sdss | 5797             | 82S                |
| 0                 | 53674.24110 | 0                 | 17.044           | 0.023             | 0.001              | 0.001              | 5.718E+02         | 1.211E+01            | 2.840E-01         | 3.688E-01         | 10                | sdss | 5797             | 82S                |
| 0                 | 53676.33207 | 1                 | 16.523           | 0.004             | 0.000              | 0.000              | 8.734E+02         | 3.218E+00            | 7.615E-02         | 9.707E-02         | 10                | sdss | 5807             | 82S                |
| 0                 | 53676.32875 | 2                 | 16.598           | 0.004             | 0.000              | 0.000              | 8.295E+02         | 3.056E+00            | 7.532E-02         | 1.051E-01         | 12                | sdss | 5807             | 82S                |
| 0                 | 53676.32958 | 3                 | 16.811           | 0.005             | 0.001              | 0.000              | 6.736E+02         | 3.102E+00            | 3.147E-01         | 1.349E-01         | 12                | sdss | 5807             | 82S                |
| 0                 | 53676.33124 | 4                 | 17.016           | 0.010             | 0.003              | 0.001              | 5.587E+02         | 5.146E+00            | 1.419E+00         | 5.661E-01         | 12                | sdss | 5807             | 82S                |
| 0                 | 53676.33041 | 0                 | 16.675           | 0.014             | 0.001              | 0.000              | 8.032E+02         | 1.036E+01            | 3.986E-01         | 3.688E-01         | 10                | sdss | 5807             | 82S                |
| ...               |             |                   |                  |                   |                    |                    |                   |                      |                   |                   |                   |      |                  |                    |

<sup>a</sup> For details of (bitwise) values see Holtzman et al. (2008). A value of 0 indicates no lines, > 1024 is very likely a bad measurement, while a value between 0 and 1024 is likely OK but frame not used for galaxy solution. <sup>b</sup> 01234 = ugriz bands. <sup>c</sup> MAG is in native SDSS photometric system, and is an asinh magnitude. No extinction correction has been applied. <sup>d</sup> Random error in magnitude. <sup>e</sup> Systematic magnitude error estimate from error in sky estimate. <sup>f</sup> Systematic magnitude error estimate from error in underlying galaxy brightness. <sup>g</sup> FLUX is in microJy using SDSS/AB correction from Holtzman et al. (2008). <sup>h</sup> Random error in flux. <sup>i</sup> Systematic flux error estimate from error in sky estimate. <sup>j</sup> Systematic flux error estimate from error in underlying galaxy brightness. <sup>k</sup> RUN gives the SDSS run identifier. <sup>l</sup> Strip gives the SDSS strip for this measurement. <sup>m</sup> NPRE gives the number of pre-SN observations used.

Note. — Data files for each supernova are published in their entirety in the electronic edition of the *Astronomical Journal*. A portion of a table is shown here for guidance regarding its form and content. The online files include some additional ancillary information about each object, including the IAU designation, the coordinates, the redshift, the expected foreground extinctions from Schlegel et al., and the derived underlying galaxy brightnesses from the scene modelling.

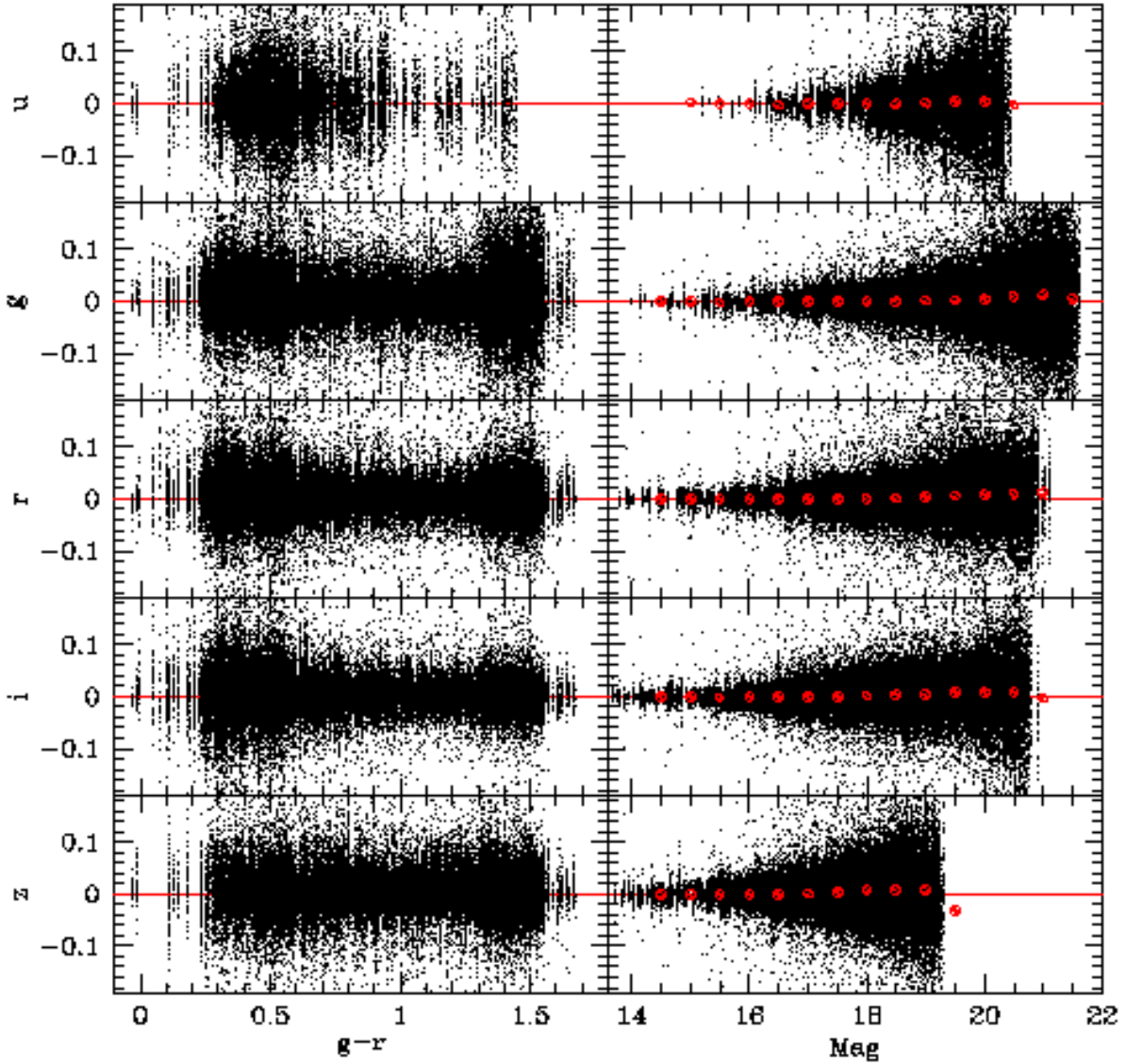


Fig. 1.— Difference between recovered stellar magnitudes and the calibration magnitudes as a function of stellar color (left panel) and stellar magnitude (right panel). This demonstrates the accuracy of our PSF photometry and also indicates typical errors as a function of stellar brightness.

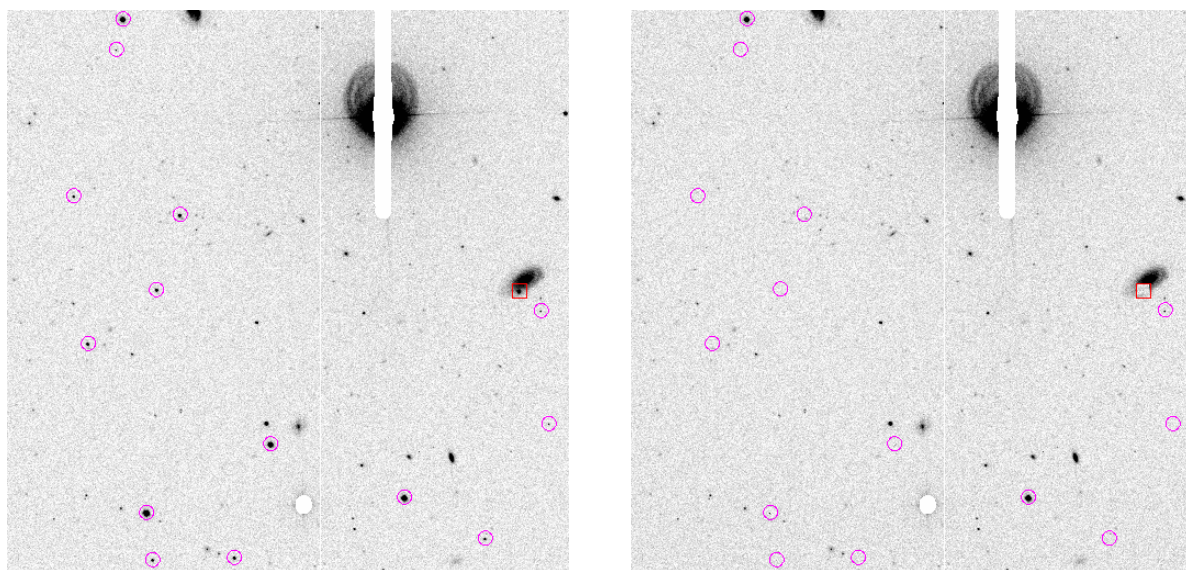


Fig. 2.— An example of an image subsection used to solve for frame parameters in the second fitting stage, *i.e.*, the astrometric solution and photometric scale factor. The stars with circles are the calibration stars used to determine the solution. The left panel shows the image before the model is subtracted, with circles around the calibration stars and a box around the supernova; the right panel shows the image after model subtraction.

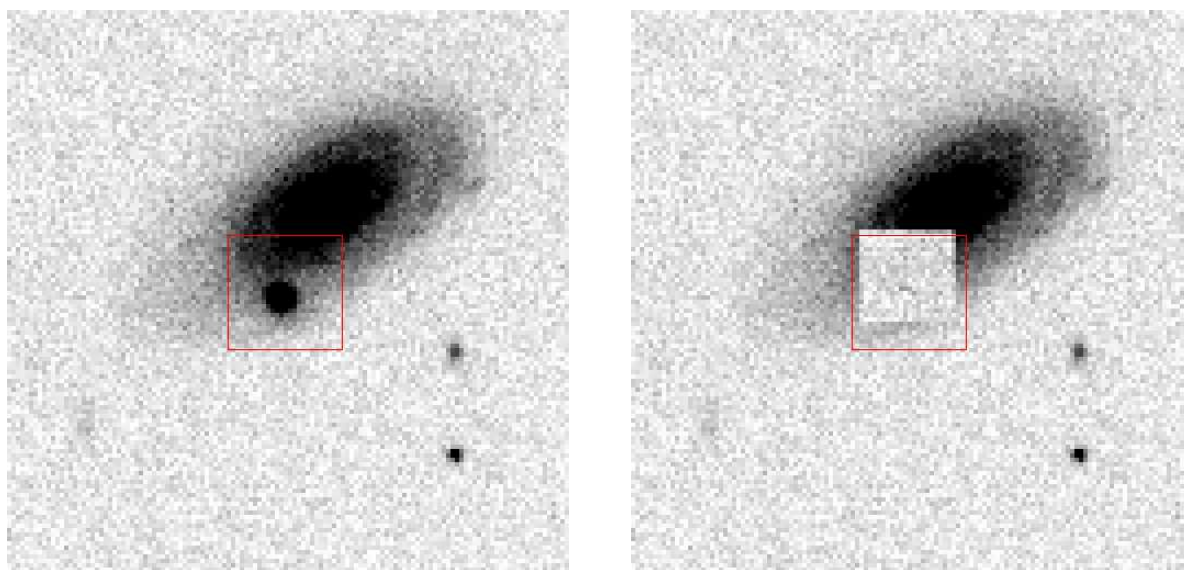


Fig. 3.— An example of an image subsection used to solve for galaxy background and supernova brightness. In this third fitting stage, an entire stack of images, including those with and without the supernovae present, are fit simultaneously. The left panel shows the image before the model is subtracted, with a box around the supernova; the right panel shows the image after model subtraction.

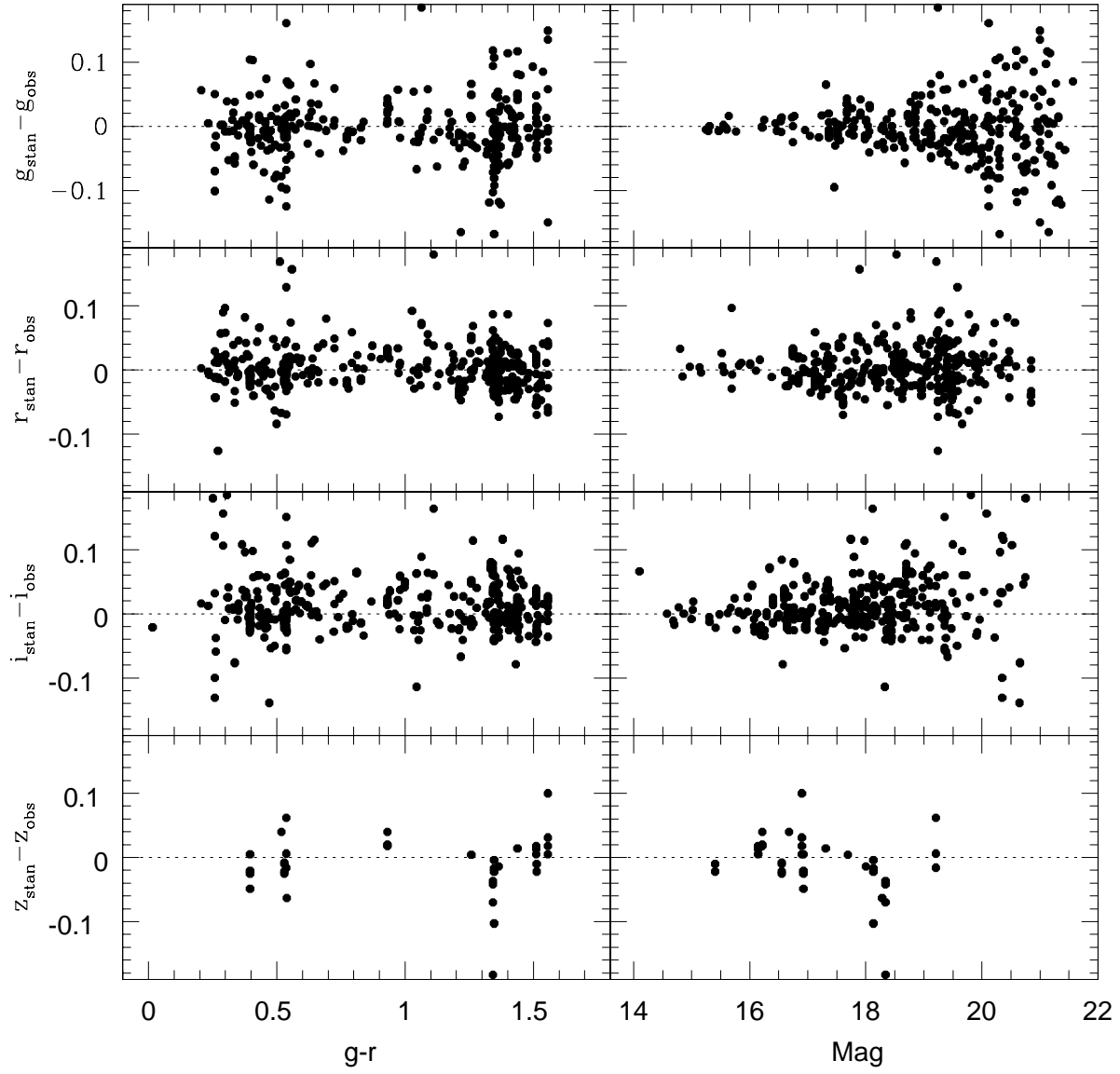


Fig. 4.— Difference between recovered and calibration photometry for calibration stars in the MDM frames, using the color terms presented in the text.



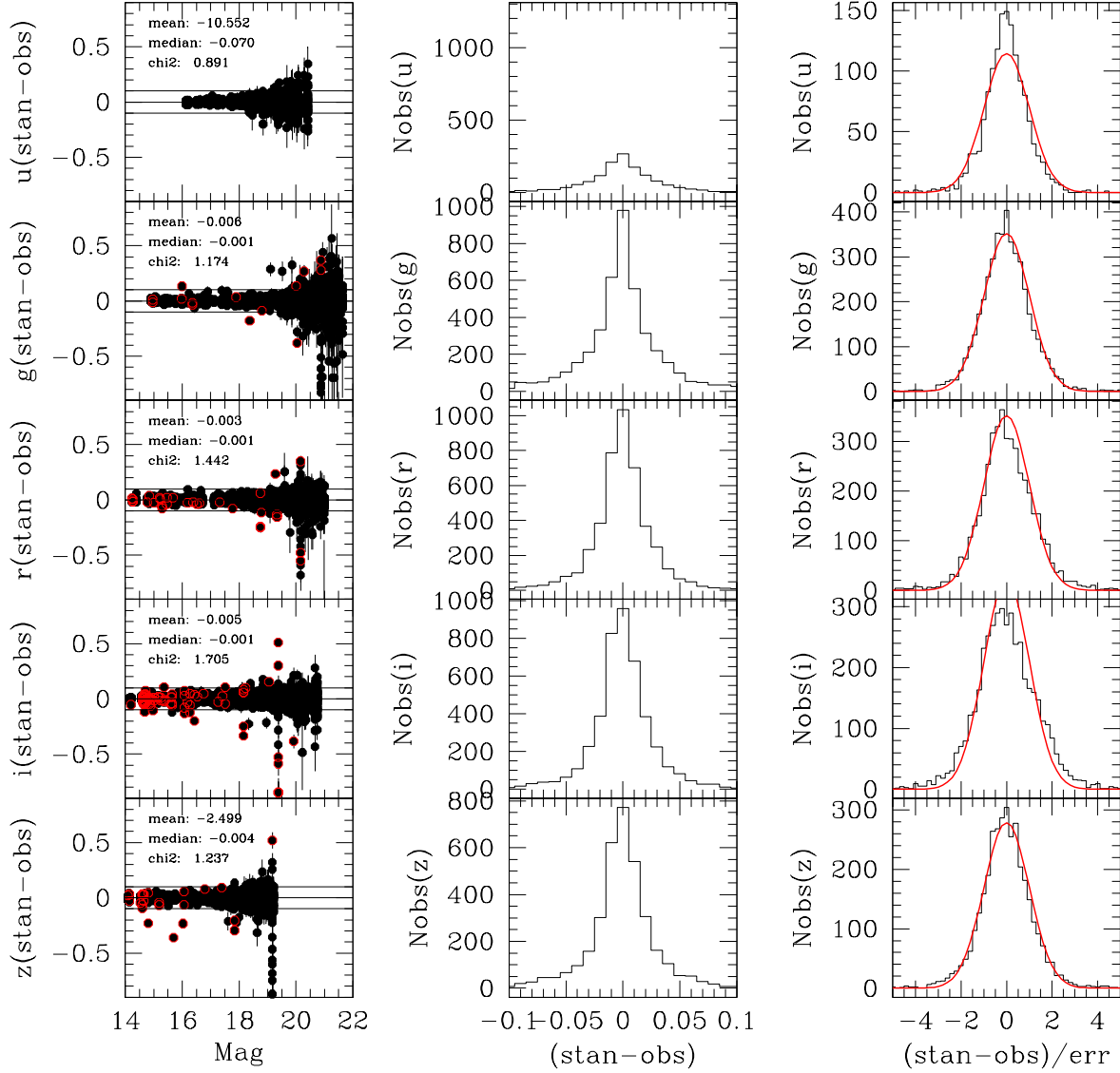


Fig. 5.— Photometry of stars near the 2005 SN, treating them as if they were supernovae, allowing for an underlying background to be fit. The left panel shows the difference between the recovered magnitude and the known stellar magnitude a function of magnitude. The central panel shows a histogram of error in the recovered magnitude, and the right panel gives a histogram of difference between recovered and calibration magnitudes, normalized by predicted photometric error. The curve in the right panel shows the expected Gaussian for the difference if the calculated errors are correct.

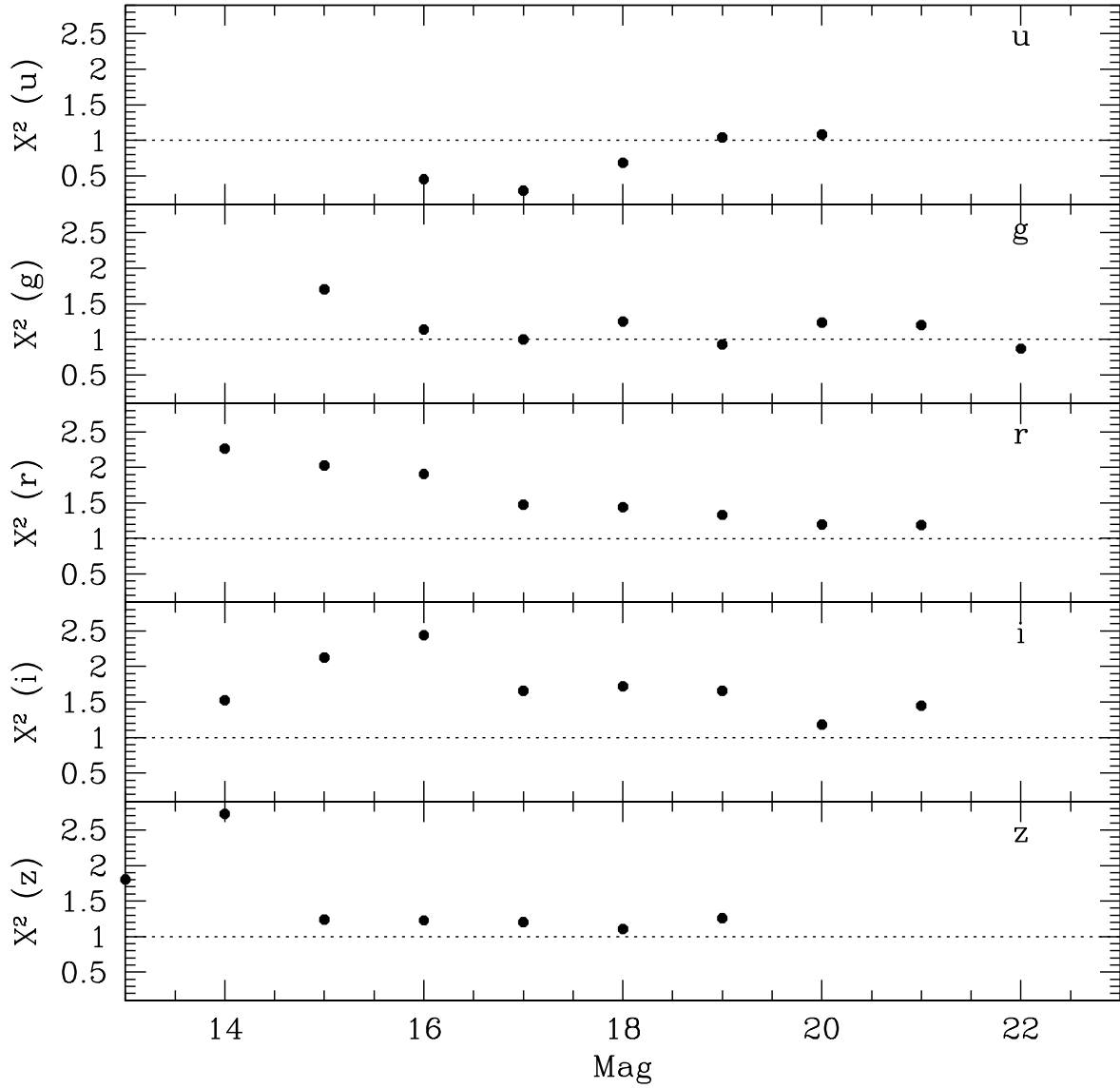


Fig. 6.— Reduced  $\chi^2$  for stars measured as if they were supernovae, computed by comparing the individual recovered magnitude against their known magnitude. No sky error term has been included.

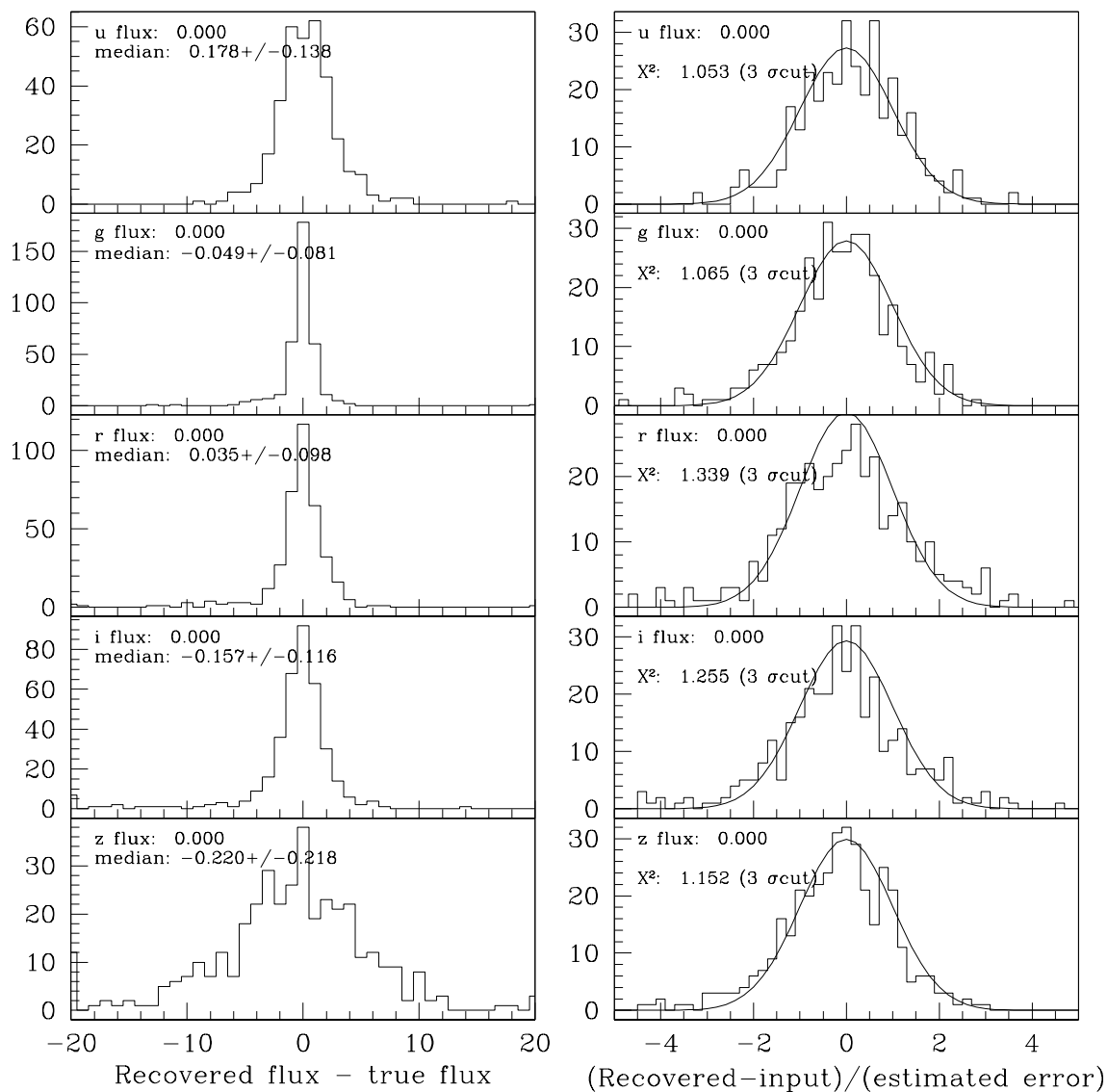


Fig. 7.— Photometry of 2005 epochs at location of 2006 supernovae, treating these as if they could have SN flux. Left panel shows histogram of recovered fluxes, which should be zero; the units are  $\mu Jy$ . The right panel shows a histogram of recovered flux normalized by predicted photometric error. The curve shows the ideal Gaussian of unit width.

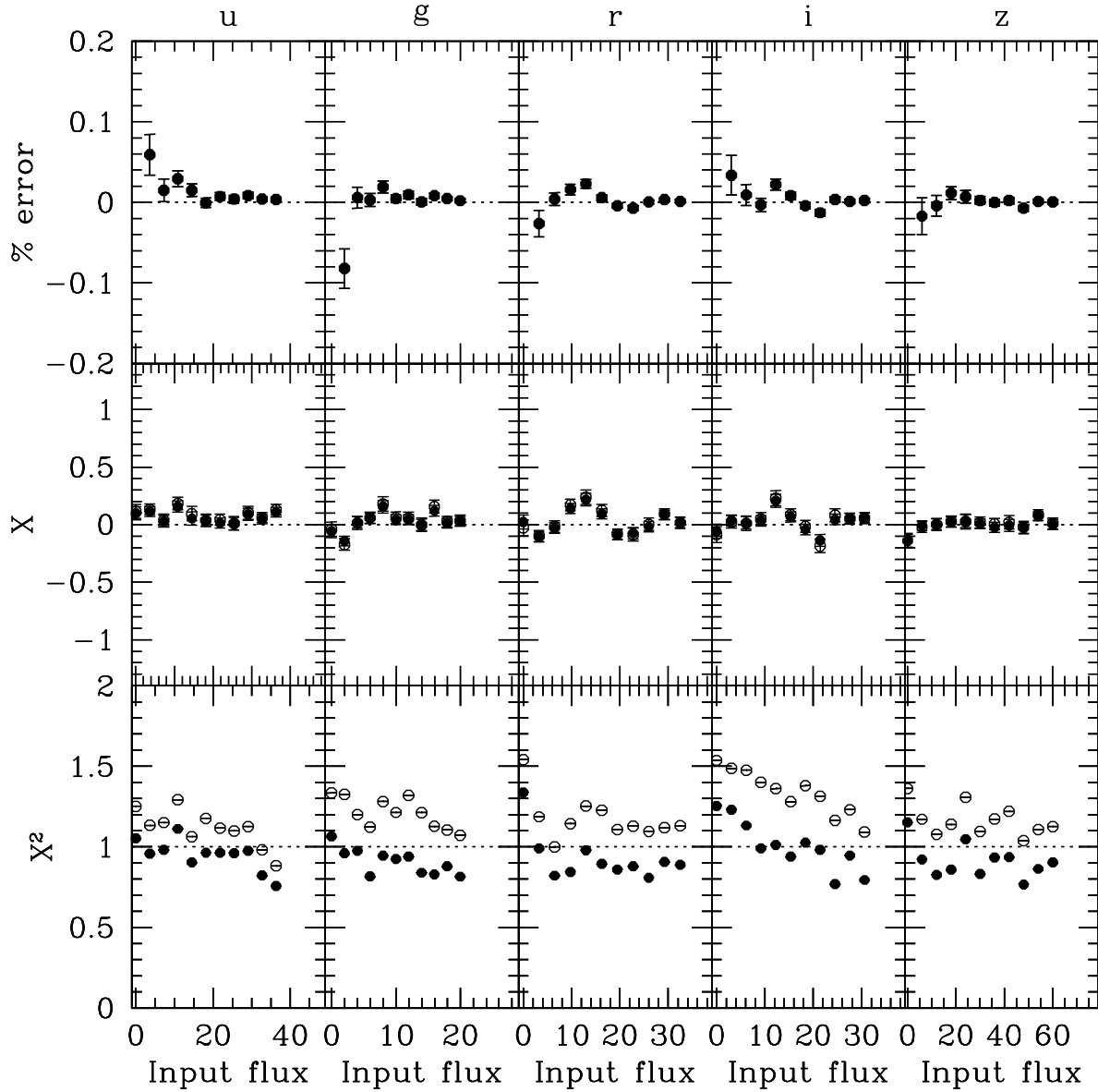


Fig. 8.— Mean recovered fluxes of artificial supernovae at a range of different input fluxes; the units are  $\mu Jy$  (note  $m = 20$  corresponds to  $36.31 \mu Jy$ ). Each point represents an average of several hundred artificial objects placed in different 2005 epochs at the location of 2006 supernovae positions. Top panels show the percent error of the recovered flux. The middle panels show the error in the derived brightness normalized by the predicted errors. The bottom panel shows the  $\chi^2$  of the recovered brightnesses; open points show the values computed using only the random error derived for the point source brightnesses, while the solid points include a term for errors in the sky level added in quadrature.

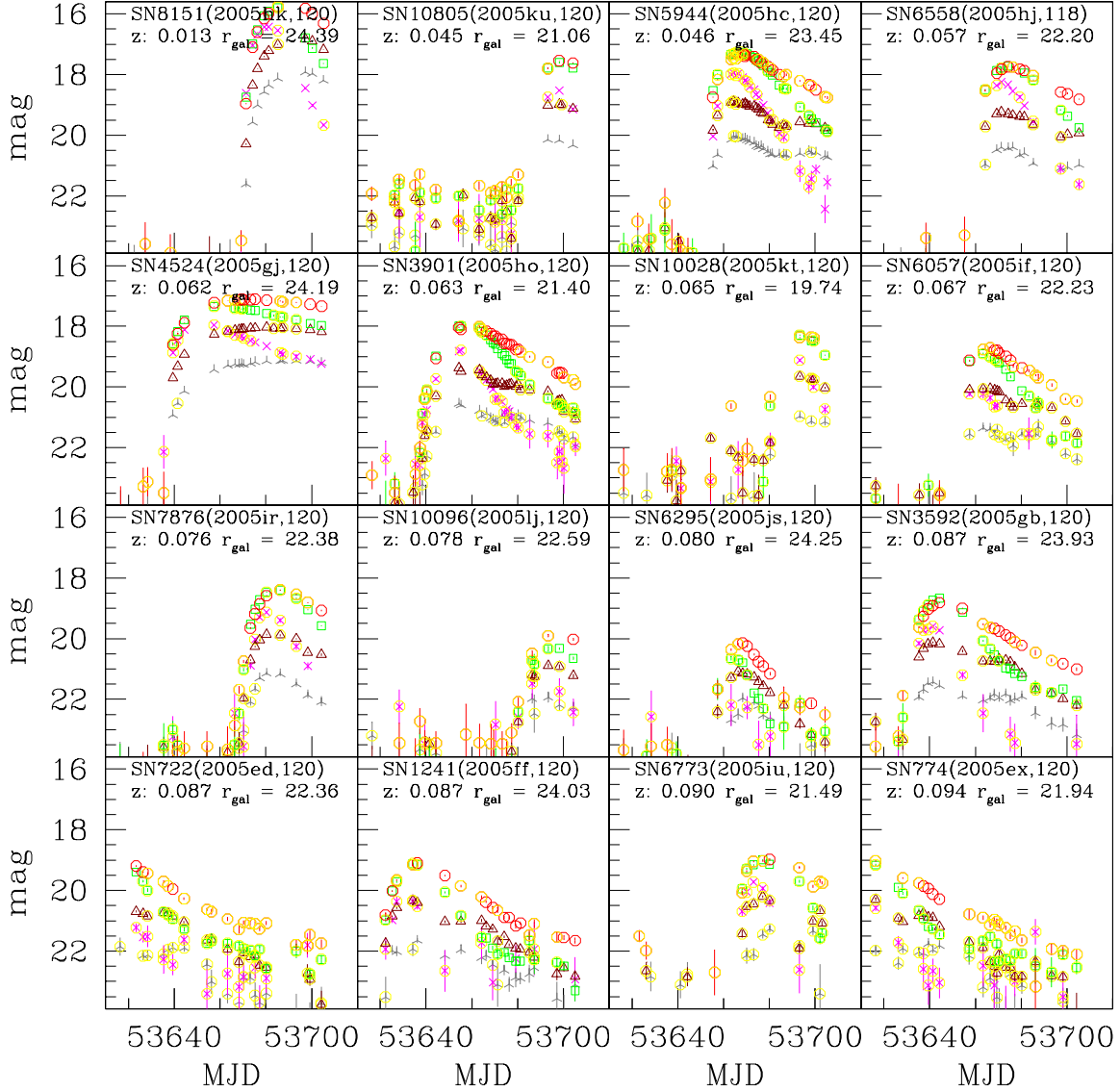


Fig. 9.— Derived light curves for the 2005 type Ia supernovae, sorted by redshift. Red points are  $r$ , green points are  $g$ , magenta points are  $u$ , brown points are  $i + 1$ , and grey points are  $z + 2$ . Points circled in yellow have non-zero photometry flags; points with flag value greater than 1024 (see text) are not plotted. The SDSS type is given, along with the IAU designation, in parentheses: type 120 are highly likely type Ia SN confirmed by the SDSS survey team, type 119 objects are probably type Ia’s, and type 118 are Ia’s confirmed by another team.

